2018 IEEE-RAS 18th International Conference on Humanoid Robots (Humanoids)
Beijing, China, November 6-9, 2018

Redundant Strain Measurement of Link Structures for Improved Stability of Light Weight Torque Controlled Robots

Hiroshi Kaminaga[1] and Fumio Kanehiro[1]

Abstract— **Robots that perform useful heavy-duty tasks are gaining attention in the field of construction, mining, and disaster recovery. For robust accomplishment of such tasks, control of interaction force is important fundamental functionality. Use of joint torque sensors is the most common method for robots that realize physical interaction. However, torque sensors add weight and reduce joint stiffness which result in loss of mobility performance. In this paper, joint torque sensing using link structure strain measurement is presented. Redundant strain gauges, placed in unstructured manner, are used to measure link deformation, which are then used to estimate all 6 components of the wrench acting on a link structure. Joint torque is then extracted from this wrench, which minimizes the cross-talks of the force measurement. Redundancy enhances the measurement accuracy and realizes fault tolerant force measurement. Simulation and experimental results of the measurement concept together with the fault recovery method are presented.**

I. Introduction

Force or torque controlled robots are gaining attention in the field of service robots including humanoid robots, which require interaction with uncertain and versatile environment and objects.

In industrial robots, wrist force / torque sensors are used to control physical interaction. Since industrial robots are used in controlled environment with known objects, wrist sensors are sufficient for measuring interaction force. Similar idea is used in locomotion stabilization in biped robots, where contact points can be limited to the end of both limbs.

This, however, is not true for robots in general environment. For such robots, contact may be multiple, spanning over multiple links of the limb. To properly control the interaction in such robots, different approach must be taken. Fig. 1 shows different types of force and torque measurement on a robot. One approach is the distributed tactile sensing. Mittendorfer et al.[1] proposed self organizing distributed tactile sensing technology. This approach is useful in delicate interaction control, but for tasks that explicitly require control of the force being transmitted, force or torque measurement in-line to the force transmission path is desirable.

Use of a joint torque sensor is the most widely used method. DLR's Light Wight Robot III[2], commercially available from KUKA, probably is the most well known and successful robot with strain gauge based torque sensors.

[1]Hiroshi Kaminaga and Fumio Kanehiro are with Humanoid Research Group, Intelligent Systems Research Institute, National Institute of Advanced Industrial Science and Technology (AIST), 1-1-1 Umezono, Tsukuba-shi, Ibaraki 305-8560, Japan hiroshi.kaminaga@aist.go.jp

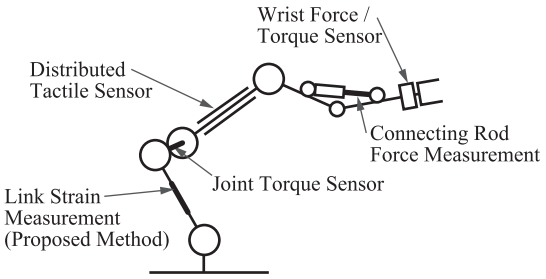

Fig. 1. Differences in Force / Torque Measurement for Force Sensitive Interaction Control

Recently, Chimp[3] and WALK-MAN[4] used relatively stiff SEAs (Series Elastic Actuators)[5] for torque sensing.

There are two large issues of the torque sensor based torque sensing. The first point is the trade-off of the control bandwidth and force sensitivity. Control bandwidth is affected both from the limited flexure stiffness and the extra weight being added from the flexure. The second point is the measurement cross sensitivity. The torque measurement is the activity of selecting one component of 6 axis force-torque wrench. This is done by measuring deformation of flexure, which has significantly lower stiffness in the direction of measurement from the other direction that are supported by bearings. Stiffer flexure is desirable from the control bandwidth point of view, but the difference of the stiffness of the flexure and bearings becomes small, which results in the measurement cross sensitivity[6].

Measuring force acting on a connecting rod of the linear actuator driven parallel link mechanism[7] enables us to eliminate necessity of extra component for torque sensing as shown in Fig. 1. Since only compression or tensile stress acts on such component, rather accurate torque can be estimated from the strain measurement with simple kinematic conversion and the cross-talk can be rejected mechanically. However, the main limitation of the method is that it can only be applied for parallel link actuated joints. It can be a large drawback for the robots that require large range of motion of the joints.

Study of exploiting redundant sensors can be found in previous works. For the case of strain gauges, Nishiwaki et al.[8] used ball-beam structure with redundant strain gauges. Lane et al.[9] used redundant strain gauge measurement spanning over multiple linkages. Tsuji and Hanyu[10] used redundant 3 axis force sensors to detect and recover defective force measurement. These studies rely on sensor placement precision, and thus are limited in the number of redundant

978-1-5386-7282-2/18/$31.00 ©2018 IEEE

TABLE I

COMPARISON OF FORCE MEASUREMENT METHOD

	Distributed Tactile Sensor	Torque Sensor	Parallel Link	Redundant Link Strain (Proposed)
Collocation with Actuators	no	yes	yes	yes
Additional Component	yes	yes	no	no
Crosstalk Rejection	yes	no	yes	yes
Actuator Dependent	no	yes	yes	no
Fault Tolerant	yes	no	no	yes

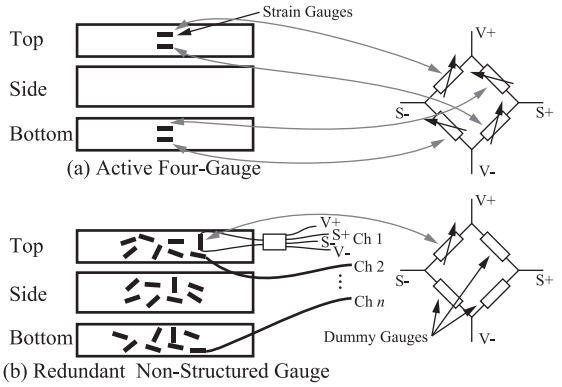

Fig. 2. The Concept of Redundant Strain Measurement Based Force Measurement

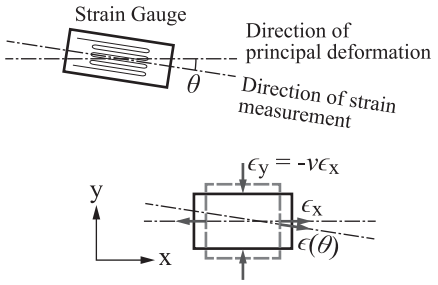

Fig. 3. Measurement Error of Strain Gauges Caused by Alignment Error and Poisson Effect

sensors.

The objective of this paper is to overcome the limitation of the methods above by measuring force acting on link structures. We propose to use redundant strain gauges on link structures with unstructured placement to enhance signal quality and fault tolerance against failures of the gauges. See Table I for the qualitative comparison of the proposed method with the other methods. With the proposed method, no additional components are necessary and no stiffness reduction will occur. Also, the proposed method is independent from the actuation method. Evolutions in the electronics enables us to treat strain gauge signals with high quality in a small circuit board, which can be connected in daisy-chain manner. It enables us to use large number of strain gauges with minimum cabling. The proposed method requires calibration of all the links, but it can be done simultaneously, since all components of the wrench are measured. This was not possible for the case of torque sensors. The placement of the strain gauges can be arbitrary as long as directional diversity is maintained. The proposed method estimates the relation of 6 axis wrench acting on a link structure from the redundant strain measurement. Joint torque is then extracted from the wrench, which results in ideal cross sensitivity decoupling. Finally, the redundancy is used to suppress the error when a strain gauge become dysfunctional. We adopt the fault detection algorithm proposed by Tsuji et al.[10] and propose the recovery algorithm that use mapping matrices with partial strains to the wrench. Simulation and experimental results are reported.

II. REDUNDANT STRAIN GAUGE MEASUREMENT

In conventional strain gauge force measurement, what is called "active four-gauge method" is used. In this method, strain gauges on antagonistic surface are connected as shown in Fig. 2. Using this method, the voltage readout becomes 4 times larger for the same stress and the thermal effect can be removed.

However, the value obtained from the four-gauge method is not yet ideal. One problem is the geometric placement error and the other is the uneven thermal effect.

To explain the first point, see Fig. 3. It is difficult to correctly place strain gauges and there exists alignment error of angle θ_e.

Strain is a tensor value and each of the inifinitesimal element is expressed with six components with regarding to a coordinate system: linear strains $(\epsilon_x, \epsilon_y, \epsilon_z)$ and torsional strains $(\gamma_{xy}, \gamma_{yz}, \gamma_{zx})$. A strain tensor T is defined as follows.

$$T = \begin{bmatrix} \epsilon_x & \frac{1}{2}\gamma_{xy} & \frac{1}{2}\gamma_{zx} \\ \frac{1}{2}\gamma_{xy} & \epsilon_y & \frac{1}{2}\gamma_{yz} \\ \frac{1}{2}\gamma_{zx} & \frac{1}{2}\gamma_{yz} & \epsilon_z \end{bmatrix} \quad (1)$$

The Poisson effect relates stress σ_i and strain ϵ_j in multiple direction. Using Poisson's ratio ν, Hooke's law can be written as follows using Young's modulus E.

$$\epsilon_x = \frac{1}{E}\{\sigma_x - \nu(\sigma_y + \sigma_z)\} \quad (2)$$

$$\epsilon_y = \frac{1}{E}\{\sigma_y - \nu(\sigma_z + \sigma_x)\} \quad (3)$$

$$\epsilon_z = \frac{1}{E}\{\sigma_z - \nu(\sigma_x + \sigma_y)\} \quad (4)$$

Hence, even when the pure stress in x direction, both ϵ_x and ϵ_y will be observed. Poisson's ratio is about 0.34 in aluminum alloys.

Poisson's ratio would cause cross sensitivity of strain in x direction for stress in other direction. For an example, strain of $-\nu\epsilon_y$ would be observed for pure y direction stress.

The strain tensor for pure x stress is given as follows.

$$T = \begin{bmatrix} \epsilon_x & 0 & 0 \\ 0 & -\nu\epsilon_x & 0 \\ 0 & 0 & -\nu\epsilon_x \end{bmatrix} \quad (5)$$

The measured strain in case of Fig. 3 is given as follows.

$$\boldsymbol{r} = \begin{bmatrix} \cos(\theta) & \sin(\theta) & 0 \end{bmatrix}^T \quad (6)$$

$$\epsilon(\theta) = \boldsymbol{r}^T T \boldsymbol{r} = \left(\cos^2(\theta) - \nu \sin^2(\theta)\right) \epsilon_{\mathrm{x}} \quad (7)$$

It would not only cause the measurement error on x axis strain, but would deviate cross sensitivity for stress in y axis direction by from $-\nu$ to $\sin^2\theta - \nu\cos^2\theta$. The error can be amplified for 4-gauge method since the error can add up with directional error of all four gauges. Thus, use of any single axis strain measurement is not suitable for measurement of strain under versatile stress conditions.

In the proposed method, multiple of Wheatstone bridge measurement with 1 strain gauge and 3 dummy gauges will be used. In this method, no alignment between gauges is necessary. Each bridge will be connected to a ratiometric AD converter in the actual implementation, which enables us to measure amount of strain with high precision under existence of noise on the power line.

Let us define a vector of strain as $\boldsymbol{\epsilon} \in \boldsymbol{R}^n$, where n is the number of strain measurements. A wrench vector at the link origin is defined as $\boldsymbol{w} \in \boldsymbol{R}^6$. When the deformation of the link is sufficiently small, stress and strain will have linear relation. Since the wrench acting on a link is a integrated value of the stress, we can assume the linear relation between the strain and the wrench.

This relation can be written as follows:

$$\boldsymbol{w} = F\boldsymbol{\epsilon} \quad (8)$$

Here, $F \in \boldsymbol{R}^{6\times n}$ is a matrix that correlates strain and wrench, which has information on Young's modulus of the link and geometric property of the strain measurement.

Let us assume the strain measurement $\boldsymbol{\epsilon}^*$ as an addition of true strain $\hat{\boldsymbol{\epsilon}}$ and Gaussian noise $\boldsymbol{x}$ with 0 average and σ standard deviation, hence:

$$\boldsymbol{\epsilon}^* = \hat{\boldsymbol{\epsilon}} + \boldsymbol{x} \quad (9)$$

The equation (8) becomes following form.

$$w_i^* = \sum_{j=1}^{n} f_{ij}\epsilon_j^* = \sum_{j=1}^{n} f_{ij}\hat{\epsilon}_j + \sum_{j=1}^{n} f_{ij}x_j \quad (10)$$

Here, the subscripts i and j indicates the row and column position of the vectors and matrices respectively. The superscript $*$ shows measured value. It is clear from (10) that if we take sufficient n, estimated wrench converges to true value under the existence of the noise.

Under the assumption of the strain-stress linearity and the noise being Gaussian, the matrix F can be identified from multiple measurements as follows:

$$F = WE^{\#} \quad (11)$$

Here, $\#$ shows the pseudoinverse of a matrix, $W = [\boldsymbol{w}_1\boldsymbol{w}_2\cdots\boldsymbol{w}_m]$ is the matrix consisting of m wrench measurements, and $E = [\boldsymbol{\epsilon}_1\boldsymbol{\epsilon}_2\cdots\boldsymbol{\epsilon}_m]$ is a matrix consisting of m strain measurements.

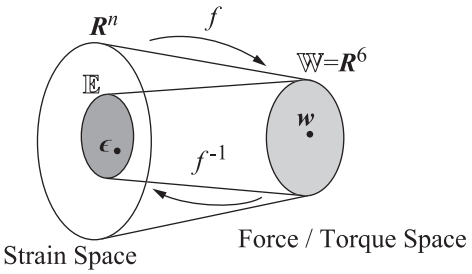

Fig. 4. Map Between Strain Space and Wrench Space

III. Fault Detection and Recovery

Although $\boldsymbol{\epsilon}$ has dimension n, there are geometric constraints that limits the value of $\boldsymbol{\epsilon}$ in subspace $\mathbb{E} \subset \boldsymbol{R}^6$ as shown in Fig. 4. In this paper, we assume the dimension of $\mathbb{E}$ to be 6. The assumption is that faulty measurements can be identified by evaluating if $\boldsymbol{\epsilon} \in \mathbb{E}$ or not.

The inverse relation of the wrench and the strain can be written as follows with $G \in \boldsymbol{R}^{n\times 6}$.

$$\boldsymbol{\epsilon} = G\boldsymbol{w} \quad (12)$$

Tsuji et al.[10] estimated G as in (13).

$$G = EW^{\#} \quad (13)$$

Let us assume $\mathbb{E}$ as $\mathbb{E} = \left\{\boldsymbol{\epsilon} \in \boldsymbol{R}^n | \boldsymbol{\epsilon} = G\boldsymbol{w}, \forall \boldsymbol{w} \in \boldsymbol{R}^6\right\}$ If a measured strain vector $\boldsymbol{\epsilon}^*$ lies within $\mathbb{E}$, then following equation should hold.

$$\boldsymbol{\epsilon}^* = GF\boldsymbol{\epsilon}^* \quad (14)$$

The outlier can be estimated by evaluating $\boldsymbol{e}$, the error between the left hand side and the right hand side.

$$\boldsymbol{e} = (I - GF)\,\boldsymbol{\epsilon}^* \quad (15)$$

Here, I is the identity matrix of appropriate dimension.

In this paper, we detected an error by evaluating $|e_i| > e_{\mathrm{th}}$. Now, the threshold e_{th} is chosen subjectively from the mean value of $|e_i|$, but clustering technique can be applied for more objective evaluation.

a) Fault Recovery Method 1 (FR1): The first method is the method proposed by Tsuji et al.[10]. In the proposed method, value of the strain gauge with fault is projected toward $\mathbb{E}$. The recovered wrench $\tilde{\boldsymbol{w}}$ is given by following equations. The index i is the estimated index of strain gauge with fault.

$$\tilde{\boldsymbol{w}} = F\tilde{\boldsymbol{\epsilon}} = F\begin{bmatrix} \tilde{\epsilon}_1 \cdots \tilde{\epsilon}_n \end{bmatrix}^T \quad (16)$$

$$\tilde{\epsilon}_i = \epsilon_i^* - \boldsymbol{e}^T \frac{\boldsymbol{q}_i}{\|\boldsymbol{q}_i\|} \quad (17)$$

where,

$$Q = \begin{bmatrix} \boldsymbol{q}_1 \cdots \boldsymbol{q}_n \end{bmatrix} = I - GF \quad (18)$$

The advantage of the method is that it minimizes computational effort by utilizing relation of the mapping shown in Fig. 4. However, since the reverse mapping G is highly redundant, it is correct only in the sense of least square.

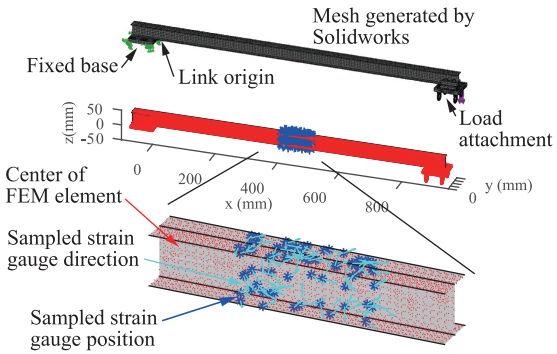

Fig. 5. Outlook, Mesh, and Simulated Strain Gauge Placement of Finite Element Analysis. The figure shows an example of 100 strain gauges.

b) Fault Recovery Method 2 (FR2): Let us define regression matrices of identification data $E_{\bar{i}_1,\cdots,\bar{i}_k}$ as E with i_1 to i_k-th row excluded. Similarly define $F_{\bar{i}_1,\cdots,\bar{i}_k}$ as follows.

$$F_{\bar{i}_1,\cdots,\bar{i}_k} = W E^{\#}_{\bar{i}_1,\cdots,\bar{i}_k} \tag{19}$$

$F_{\bar{i}_1,\cdots,\bar{i}_k}$ can be calculated off-line.

The recovered wrench data $\tilde{\boldsymbol{w}}$ is given as follows with i_1 to i_k being the index of the element detected by $|e_{i_k}| > e_{\rm th}$.

$$\tilde{\boldsymbol{w}} = F_{\bar{i}_1,\cdots,\bar{i}_k} \boldsymbol{\epsilon}_{\bar{i}_1,\cdots,\bar{i}_k} \tag{20}$$

Here,$\boldsymbol{\epsilon}_{\bar{i}_1,\cdots,\bar{i}_k}$ is the vector of strain measurement with i_1 to i_k-th row excluded.

The advantage of the method is that if the index of the dysfunctional strain gauge was correctly detected, recovered data should be optimal in the sense of least square. The drawback of the method is that although $F_{\bar{i}_1,\cdots,\bar{i}_k}$ can be calculated off-line it is not realistic to calculate exhaustive combination of excluded indices, since the number of matrices will grow exponentially with k.

However, the most likely case of the failure is single strain gauge becoming dysfunctional. Hence, the realistic approach is to expect single failure, and perform maintenance after the operation if a failure was detected.

IV. Simulation

Simulation of the proposed method was carried out using finite element analysis (FEA) of CAD software. H-shaped cantilever beam was used as the specimen to see the directional effect, which cannot be observed with a cylindrical beam. Position of the strain measurement was chosen to be around the center of the beam. Position of the gauges were randomly sampled from the position of the mesh data obtained from FEA result. Fig. 5 shows setup used for the simulation. Fig. 6 shows dimension of the flange for load attachment. Eyebolts for load connection are attached to $\boldsymbol{p}_0 \rightarrow \boldsymbol{p}_3$.

Direction of the strain gauges on the measurement surface was expressed as angle $\boldsymbol{\theta} \in \boldsymbol{R}^n$ with the x axis direction. Each element of the $\boldsymbol{\theta}$ was randomly sampled from $\theta_i \in (-\pi/2, \pi/2]$ with the uniform distribution.

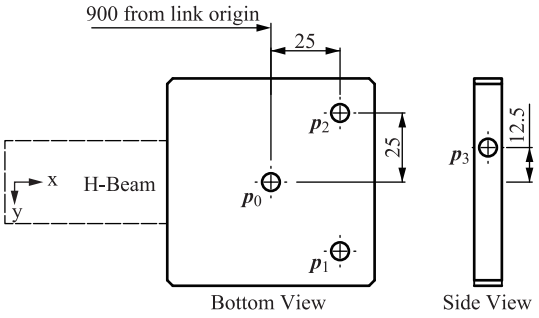

Fig. 6. Load Attachment Dimension

TABLE II
Training Data Set

Set	f_x	f_y	f_z	m_x	m_y	m_z
	N			Nm		
1	20	0	0	0	-100e-3	0
2	10	0	0	0	-50e-3	-125e-3
3	10	0	0	0	-50e-3	125e-3
4	0	10	0	50e-3	0	8875e-3
5	0	10	0	50e-3	0	9125e-3
6	0	0	40	0	36000e-3	0
7	0	0	10	-250e-3	9250e-3	0
8	0	0	10	-250e-3	8750e-3	0
9	0	0	10	250e-3	9250e-3	0

Strain results of the FEA are given as linear strains $(\epsilon_{\rm x}, \epsilon_{\rm y}, \epsilon_{\rm z})$ and torsional strains $(\gamma_{\rm xy}, \gamma_{\rm yz}, \gamma_{\rm zx})$ regarding the Cartesian coordinate X, Y, Z. To convert these values to the strain gauge measurements, following tensor conversion was used.

$$\epsilon = \boldsymbol{r}^T T \boldsymbol{r} \tag{21}$$

$$T = \begin{bmatrix} \epsilon_{\rm x} & \frac{1}{2}\gamma_{\rm xy} & \frac{1}{2}\gamma_{\rm zx} \\ \frac{1}{2}\gamma_{\rm xy} & \epsilon_{\rm y} & \frac{1}{2}\gamma_{\rm yz} \\ \frac{1}{2}\gamma_{\rm zx} & \frac{1}{2}\gamma_{\rm yz} & \epsilon_{\rm z} \end{bmatrix} \tag{22}$$

$$\boldsymbol{r} = \begin{cases} \begin{bmatrix} \cos(\theta) & -\sin(\theta) & 0 \end{bmatrix}^T & \text{(xy plane)} \\ \begin{bmatrix} \cos(\theta) & 0 & \sin(\theta) \end{bmatrix}^T & \text{(xz plane)} \end{cases} \tag{23}$$

To evaluate effect of the measurement noise, Gaussian noise x was applied as follows:

$$\epsilon^* = \epsilon + x \tag{24}$$

To evaluate the effect of the defective strain gauges, an element of $\boldsymbol{\epsilon}^*$ as randomly selected and replaced with fault value $\epsilon_{\rm f}$ as $\epsilon^*_i = \epsilon_{\rm f}$.

To identify the matrix F, data shown in Table II were used. The direction and magnitude of the applied force was chosen to give sufficient excitation to all 6 components of the wrench. To evaluate the wrench estimation performance,

TABLE III
Cross Validation Data Set

Set	f_x	f_y	f_z	m_x	m_y	m_z
	N			Nm		
1	0	20	0	100e-3	0	18000e-3
2	0	0	10	250e-3	8750e-3	0

TABLE IV

PERFORMANCE EVALUATIONS FOR 100 GAUGES(%): (3-X) SHOWS THE RESULT FOR $\epsilon_{\mathrm{f}} = 0\mu\varepsilon$. (4-X) SHOWS THE RESULT FOR $\epsilon_{\mathrm{f}} = 1000\mu\varepsilon$

Type	Data Set	Mean	Max	Std. Dev.
(1)	1	1.600e-3	1.600e-3	-
No noise	2	0.1258	0.1258	-
(2)	1	14.66	54.78	9.182
Noise ($\sigma = 1\mu\varepsilon$)	2	29.69	111.0	18.59
(3-1)	1	87.42	445.9	75.42
Fault (0 $\mu\varepsilon$)	2	97.75	451.9	88.69
(3-2)	1	67.72	260.8	55.38
Fault recovery 1	2	97.75	451.9	88.69
(3-3)	1	14.76	53.46	9.273
Fault recovery 2	2	29.91	108.1	18.70
(4-1)	1	1467	5001	1033
Fault ($1000\mu\varepsilon$)	2	2937	10370	2151
(4-2)	1	66.17	545.3	89.77
Fault recovery 1	2	130.2	1224	180.2
(4-3)	1	14.71	53.46	9.261
Fault recovery 2	2	29.77	108.1	18.75
(5)	1	14.71	53.46	9.261
Ideal recovery	2	29.77	108.1	18.75

data shown in Table III are used for cross validation. Table IV shows the result for the case of 100 strain gauges. Standard deviation of the noise was chosen to be $1\mu\varepsilon$, which is roughly 10% of the measured strain. Throughout the paper, we use the unit ε to indicate the amount of the strain, hence $1\mu\varepsilon = 10^{-6}\varepsilon$.

The error of the result was evaluated as a norm of a error vector $\boldsymbol{e}_{\mathrm{w}}$ defined as follows.

$$\boldsymbol{e}_{\mathrm{w}} = \frac{\boldsymbol{w}^* - \hat{\boldsymbol{w}}}{\|\hat{\boldsymbol{w}}\|} \tag{25}$$

Here, let us define $\hat{\boldsymbol{w}}$ and $\boldsymbol{w}^* = F\boldsymbol{\epsilon}^*$ as the true value and the estimated value of the wrench respectively. Mean value, maximum value, and standard deviation are calculated for $\|\boldsymbol{e}_{\mathrm{w}}\|$.

The ideal fault recovery data was obtained by FR2 method in the previous section with the known faulty strain gauge index.

Table IV and Fig. 7 shows the cross validation simulation result for the case of 100 randomly placed strain gauges. Data set shows the index of the data set shown in Table III. Independent 1000 samples of the Gaussian noise were applied to all the gauges to obtain statistical data. Strain gauge with fault was selected randomly in each trial, with uniform distribution.

From the result, the wrench can be estimated with limited error for the case with no noise and the data with Gaussian noise. The error becomes large in the case with strain gauge fault, but both the recovery methods suppress fault effectively. The error of FR2 became 24% of that of FR1, which shows efficacy of FR2.

Next, the effect of noise on each component of the estimated wrench and the number of strain gauges were evaluated. Table V and Fig. 8 shows the simulated result. From the result, we can see relatively large noise effect on f_{x} (force in x direction). This is due to the stiffness. The noise is multiplied in the direction of high stiffness.

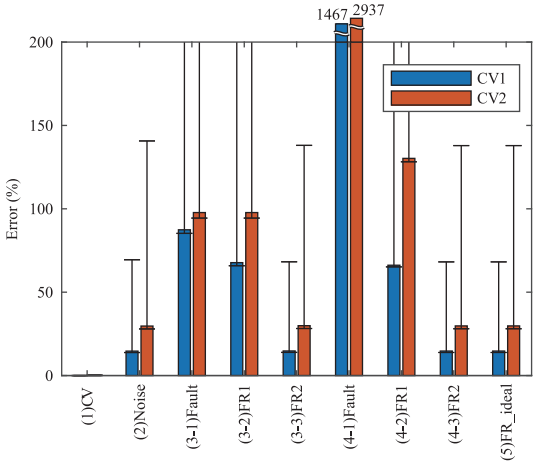

Fig. 7. Simulation Result for 100 Strain Gauges(%). (3-x) shows the result for $\epsilon_{\mathrm{f}} = 0\mu\varepsilon$. (4-x) shows the result for $\epsilon_{\mathrm{f}} = 1000\mu\varepsilon$

TABLE V

NOISE SUPPRESSION PERFORMANCE OF STRAIN GAUGE REDUNDANCY

n	Direction	Error Standard Deviation		
		x	y	z
100	Force (N)	1.801	0.3221	0.4454
	Moment (Nm)	4.942e-3	0.2118	0.1504
50	Force (N)	3.040	0.5830	0.7089
	Moment (Nm)	8.796e-3	0.3394	0.2737
20	Force (N)	5.759	0.9339	1.461
	Moment (Nm)	14.08e-3	0.6812	0.4369
10	Force (N)	86.03	8.075	8.745
	Moment (Nm)	0.1418	5.973	4.015

The noise is suppressed almost linearly with the number of gauges in the range of 20 to 100. There is a large jump from the data of 20 and 10. From the evaluation, number of strain gauges above 20 is realistic. In this range, number of strain gauges and the noise suppression performance are in linear trade-off condition.

V. EXPERIMENT

The preliminary experiments were carried out for the proof of the concept. In the experiment, 8 strain gauges were applied on the top surface of the H beam and the bottom surface as shown in Fig. 9. Although the analysis in the previous section indicated the use of more than 20 gauges is desirable, the number of strain gauges was limited by the number of strain measurement channels of the AD converter, which will be resolved in future studies. The effectiveness of the redundancy can still be evaluated, with the limited noise suppression performance.

The bias and noise power were measured at rest configuration (external force = 0). Table VI shows the result. From this result, standard deviation of the noise acting on each strain gauge is about $1\mu\varepsilon$, which is roughly the value that is evaluated in the simulation.

The gain shown in Table VII are used in the identification of F. Let us define the force value measured by the force gauge as f. The truth data of the wrench is calculated by

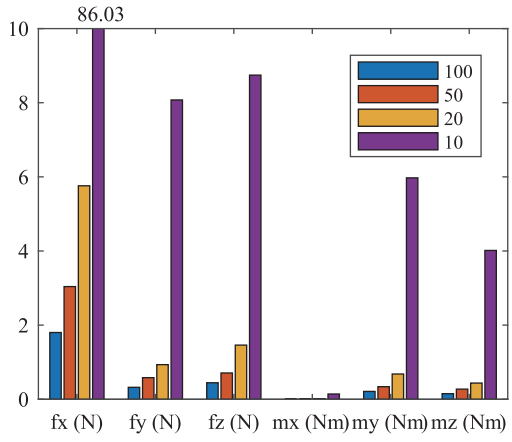

Fig. 8. Effect of Noise on Each Component of Wrench and Number of Strain Gauges

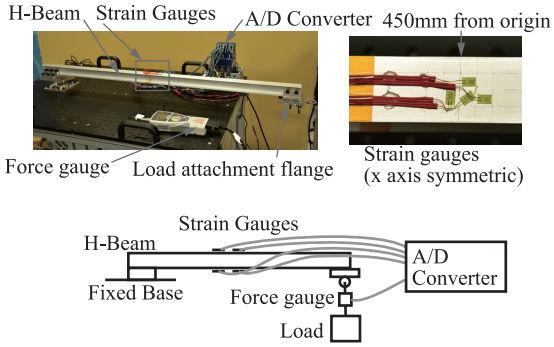

Fig. 9. Experiment Setup

following equation.

$$\boldsymbol{w} = \boldsymbol{g}\,(f + f_{\mathrm{o}}) \tag{26}$$

Here, f_{o} is a value that compensates for the weight of the force gauge, which are applied to the z-direction data with the value of 80grams. $\boldsymbol{g}$ is the conversion column vector that consist of row data shown in Table VII.

Similarly, truth data for cross validation was generated using gain data shown in Table VIII.

The experimental result is shown in Table IX. The data was collected at 25kHz, and the data shown here are unfiltered. Data set 4 contains data with a strain gauge disconnected. The result shows relatively large noise on f_{x},

TABLE VI

BIAS AND NOISE MEASUREMENT OF STRAIN GAUGES

Gauge ID	Mean ($\mu\varepsilon$)	Standard Deviation ($\mu\varepsilon$)
1	-757.0	1.001
2	-1241	1.004
3	-1487	1.024
4	313.7	1.021
5	-1100	0.9927
6	-926.3	0.9981
7	-1493	1.011
8	-1587	0.9940

TABLE VII

TRAINING DATA GAIN USED IN EXPERIMENT

Set	f_x	f_y	f_z	m_x	m_y	m_z
				m		
1	1	0	0	0	-10e-3	12.5e-3
2	0	-1	0	-35e-3	0	-925e-3
3	0	0	-1	0	900e-3	0
4	0	0	-1	-25e-3	925e-3	0
5	0	0	-1	25e-3	925e-3	0
6	0	0	-1	0	900e-3	0

TABLE VIII

CROSS VALIDATION DATA GAIN USED IN EXPERIMENT

Set	f_x	f_y	f_z	m_x	m_y	m_z
				m		
1	1	0	0	0	-35e-3	25e-3
2	0	-1	0	-35e-3	0	-900e-3
3	0	0	-1	-25e-3	925e-3	0
4	0	0	-1	0	900e-3	0

which was already expected from the simulation, but other components show small error and noise. In reality, when the data is used for torque control, the component of the force that is to be used will be either m_{x}, m_{y}, or m_{z}. Also, from the result, fault recovery is not causing a harm in the result of the data set without strain gauge fault. For the actual fault recovery, FR1 shows limited performance, but FR2 shows signal error almost comparable to that of the case without a fault.

Fig. 10 shows the time series data of data set 4. Note that in all figures, estimated wrench with fault signal are completely out of the range. Except for the graph of m_{x}, FR1 is also out of the range. For the graphs except for f_{x}, truth and FR2 values overlap. From this graph, two results were obtained. 1) Proposed method show good match with the truth (f_{x}: 3% error, 11% noise) 2) Proposed fault recovery method show only small remaining error.

VI. CONCLUSIONS

In this paper, link strain measurement for force control and joint torque control was presented. Redundant strain gauges were placed in unstructured manner to improve signal quality and fault tolerant behavior. Fault recovery method using partial mapping matrix was proposed.

From the simulation, the concept of the redundant measurement and fault recovery methods were verified statistically with randomly sampled strain gauge position and direction. The simulation result indicated that the force measurement in beam compression directions tend to be noisy due to the stiffness in the direction of the measurement. Also, the simulation indicated the use of more than 20 strain gauges is desirable from the signal quality point of view.

In the experiment, due to the equipment limitation, only 8 strain gauges were used. Still, the estimated wrench from the 8 strain gauges showed good match with the truth. The force in the direction of beam compression (f_{x}) showed the worst signal accuracy and noise, but still the error was 3% for the accuracy, and 11% noise. Since the result here

TABLE IX

ERROR ANALYSIS OF THE EXPERIMENT

Data Set	Error Mean						Error Standard Deviation					
	f_x (N)	f_y (N)	f_z (N)	m_x (Nm)	m_y (Nm)	m_z (Nm)	f_x (N)	f_y (N)	f_z (N)	m_x (Nm)	m_y (Nm)	m_z (Nm)
1	-1.717	-2.366	4.405	-0.04310	-2.925	-0.5930	3.516	0.8257	1.675	0.01825	1.117	0.3715
FR1	-1.717	-2.366	4.405	-0.04310	-2.925	-0.5930	3.516	0.8257	1.675	0.01825	1.117	0.3715
FR2	-1.717	-2.366	4.405	-0.04310	-2.925	-0.5930	3.516	0.8257	1.675	0.01825	1.117	0.3715
2	1.248	-0.6729	0.3170	-0.1063	-0.2998	-0.8105	3.855	0.4797	0.1158	0.02040	0.09038	0.4385
FR1	1.248	-0.6729	0.3170	-0.1063	-0.2998	-0.8105	3.855	0.4797	0.1158	0.02040	0.09038	0.4385
FR2	1.248	-0.6729	0.3170	-0.1063	-0.2998	-0.8105	3.855	0.4797	0.1158	0.02040	0.09038	0.4385
3	0.9815	0.01239	0.2298	0.006294	-0.2912	0.02373	3.440	0.2351	0.4813	0.02103	0.4467	0.2324
FR1	0.9815	0.01239	0.2298	0.006294	-0.2912	0.02373	3.440	0.2352	0.4813	0.02103	0.4467	0.2324
FR2	0.9815	0.01239	0.2298	0.006294	-0.2912	0.02373	3.440	0.2352	0.4813	0.02103	0.4467	0.2324
4	-74090	-4050	2496	-19.01	-1701	-4672	106.1	5.528	4.816	0.03154	3.361	6.440
FR1	-23370	-1278	788.1	-6.024	-537.2	-1474	102.1	5.307	4.680	0.03053	3.269	6.183
FR2	15.35	0.1142	0.7956	-0.03824	-0.4833	0.2975	4.408	0.2594	1.388	0.007730	1.047	0.2461

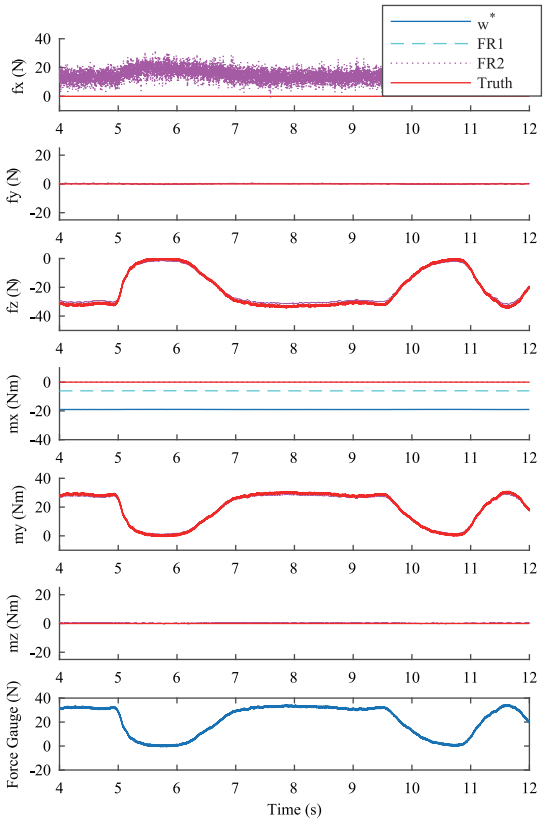

Fig. 10. Estimated (w^*), Recovered (FR1 and FR2), and Truth for Data Set 4 (Strain Gauge 6 Disconnected). Note that direct estimation with fault and FR1 data are plotted out of the range where the truth and FR2 plots overlap in f_y, m_x, m_y, and m_z.

weren't filtered, filtering would significantly improve the signal quality. Both from the simulation and the experiment, fault recovery with partial mapping matrix (FR2) showed significantly lower recovery error than the previously proposed method for redundant force measurement[10].

Current limitation of the method is the cancellation of the temperature effect. This can be resolved by including the temperature data for calculation of mapping matrix F, but it would require more redundancy of strain gauges that what we have presented in this paper. Implementation of distributed strain gauge electronics and use of more redundant gauges are in the scope of the future studies.

REFERENCES

[1] P. Mittendorfer, E. Yoshida, and G. Cheng, "Realizing whole-body tactile interactions with a self-organizing and multi-modal artificial skin on a humanoid robot," *Advanced Robotics*, vol. 1, no. 29, pp. 51–67, 2015.

[2] G. Hirzinger, N. Sporer, A. Albu-Schäffer, M. Hahnle, R. Krenn, A. Pascucci, and M. Schedl, "DLR's torque-controlled light weight robot III - are we reaching the technological limits now?" in *Proc. Int. Conf. Robotics and Automation*, 2002.

[3] A. Stentz, H. Herman, A. Kelly, E. Meyhofer, G. C. Haynes, D. Stager, B. Zajac, J. A. Bagnell, J. Brindza, C. Dellin, M. George, J. Gonzalez-Mora, S. Hyde, M. Jones, M. Laverne, M. Likhachev, L. Lister, M. D. Powers, O. Ramos, J. Ray, D. P. Rice, J. Scheifflee, R. Sidki, S. Srinivasa, K. Strabala, J. P. Tardif, J.-S. Valois, J. M. Vandeweghe, M. D. Wagner, and C. Wellington, "CHIMP, the CMU highly intelligent mobile platform," *J. Field Robotics*, vol. 32, no. 2, pp. 209–228, 2015.

[4] N. G. Tsagarakis, D. G. Caldwell, F. Negrello, W. Choi, L. Baccelliere, V. Loc, J. Noorden, L. Muratore, A. Margan, A. Cardellino, L. Natale, E. M. Hoffman, H. Dallali, N. Kashiri, J. Malzahn, J. Lee, P. Kryczka, D. Kanoulas, M. Garabini, M. Catalano, M. Ferrati, V. Varricchio, L. Pallottino, C. Pavan, A. Bicchi, A. Settimi, A. Rocchi, and A. Ajoudani, "WALK-MAN: A high performance humanoid platform for realistic environments," *J. Field Robotics*, 2017.

[5] G. A. Pratt and M. M. Williamson, "Series elastic actuators," in *Proc. Int. Conf. Intelligent Robots and Systems*, 1995, pp. 399–406.

[6] H. Kaminaga, K. Odanaka, T. Kawakami, and Y. Nakamura, "Measurement crosstalk elimination of torque encoder using selectively compliant suspension," in *Proc. Int. Conf. Robotics and Automation*, 2011, pp. 4774–4779.

[7] H. Kaminaga, T. Ko, S. Yorita, S. Sato, R. Masumura, M. Komagata, T. Ishikawa, T. Miyatake, and Y. Nakamura, "Enhancement of mechanical strength, computational power, and heat management for fieldwork humanoid robots," in *Proc. Int. Conf. Humanoid Robots*, 2016, pp. 786–793.

[8] K. Nishiwaki, Y. Murakami, S. Kagami, Y. Kuniyoshi, M. Inaba, and H. Inoue, "A six-axis force sensor with parallel support mechanism to measure the ground reaction force of humanoid robot," in *Proc. Int. Conf. on Robotics and Automation*, 2002, pp. 2277–2282.

[9] D. M. Lane, J. B. C. Davies, G. Robinson, D. J. OfBrien, J. Sneddon, E. Seaton, and A. Elfstrom, "The AMADEUS dextrous subsea hand: Design, modeling, and sensor processing," *IEEE J. Oceanic Eng.*, vol. 24, no. 1, pp. 96–111, 1999.

[10] T. Tsuji and R. Hanyu, "Fault tolerance measurement using a six-axis force/torque sensing system with redundancy," in *Proc. IEEE Int. Conf. Intelligent Robots and Systems*, 2010, pp. 1890–1895.